Bollettino di Geofisica Teorica ed Applicata Vol. 61, n. 4, pp. 487-498; December 2020
DOI 10.4430/bgta0334

Application of Riesz Transform to the aeromagnetic data of the central In Ouzzal terrane and adjacent zone, southern Algeria

L. Harrouchi[1], M.-C. Berguig[2], R. Boutrika[1], M. Hamoudi[2] and A. Bendaoud[3]

[1] *Sahara Geology Laboratory, Kasdi Merbah University, Ouargla, Algeria*
[2] *Geophysics Laboratory and Geophysics Department, FSTGAT/USTHB, Algiers, Algeria*
[3] *Geology Department, FSTGAT/USTHB, Algiers, Algeria*

(Received: 30 May 2019; accepted: 20 May 2020)

ABSTRACT The main objective of this work is to interpret aeromagnetic data of the central In Ouzzal terrane and adjacent zone, southern Algeria using the Riesz Transform (RT) method. In this paper, we developed the RT method using the concepts of monogenic functions with Cauchy Riemann conditions. The result, obtained by calculation, led us to the new expression of the Riesz Analytic Signal Amplitude (RASA) and Riesz Local Phase (RLP), respectively. Tests on a synthetic magnetic model showed that the RASA and RLP had a better performance in delineating the geological contacts that were not seen in the original data. The advantage of this RT method is that it is less sensitive to noise. By applying the Euler deconvolution method using the RASA to the aeromagnetic data of the study area, we obtained the West Ouzzalian Fault (WOF), which is below the Paleozoic cover and has a depth of 0.8 km. At a distance of 30 km from the WOF, we find the East Ouzzalian Fault (EOF) with a depth of about 5 km. According to the RLP, the dip of the WOF, the EOF and the Adrar Fault are vertical. The fault systems located inside of the central In Ouzzal terrane are, generally, inclined towards the west.

Key words: Riesz Transform, Riesz Analytic Signal Amplitude, Riesz Local Phase, Euler deconvolution, aeromagnetic data, In Ouzzal terrane.

1. Introduction

Nabighian (1984) established the relationship between the horizontal and the vertical derivatives in the 3D analytic signal by using the fundamental property of Hilbert Transform (HT). The HT may have become the most important mathematical tool to define the analytic signal (Li and Pilkington, 2016). Later, Roest *et al*. (1992) showed that it is possible to apply this method to 3D structures and defined the Analytic Signal Amplitude (ASA) as being the square root of the sum of squares of both horizontal and vertical derivatives of a magnetic anomaly. Büllow (1999) proposed a pattern of a 2D signal built in the algebra of quaternions, which generalises in an elegant and subtle way the notions of analytic signal and local phase. Constructing new signals using different transforms, like the Riesz Transform (RT) for the monogenic signal (Felsberg and Sommer, 2001; Hassan and Yalamanchili, 2013; Hidalgo-Gato and Barbosa, 2015; Li and Pilkington, 2016) is an ongoing process trying to extract all the hidden pertained information related to causative sources.

The main objective of this work is to interpret magnetic data using the RT method. The RT method, so named after the mathematician Riesz (1928), has long been the multidimensional nD extension of the Hilbert transformation (Stein and Weiss, 1971). In this paper, we developed the RT method using the concepts of monogenic functions with Cauchy-Riemann conditions. The computational results lead us to the general mathematical formulation of the analytical signal in *n*-dimensional space. From the latter formula, we obtained a new expression of the Riesz Analytic Signal Amplitude (RASA) and the Riesz Local Phase (RLP), respectively. In this present study, we apply the Euler Deconvolution (ED) method using RASA to the example of synthetic data and to the aeromagnetic data of the central In Ouzzal terrane and adjacent zone.

The ED method is based on a mathematical process represented by Euler's homogeneity equation defined by (Thompson, 1982; Reid *et al*., 1990):

$$(x - x_0)\partial T/\partial x + (y - y_0)\partial T/\partial y + (z - z_0)\partial T/\partial z = N(B - T) \tag{1}$$

where $(\partial T/\partial x, \partial T/\partial y, \partial T/\partial z)$ are first order derivatives of the potential field T in the x, y and z directions, respectively. (x_0, y_0, z_0) are the source location Cartesian coordinates and B is the regional value of the Total Field; N is the Euler's Structural Index (SI) which characterises the source geometry. The SI categorises the anomaly attenuation rate at the observation point and depends on the source geometry, where it varies from 0 to 3. Detailed numerical development may be found in Reid *et al*. (1990). In this study, the ED method with RASA was calculated using the ED software (Durrheim and Cooper, 1998).

2. Methodology

2.1. nD Riesz Transform

Let us consider a derivation function $f(X_{n+1})$ with $(n + 1)$D such as:

$$f(X_{n+1}) = \left[f_1(X_{n+1}), f_2(X_{n+1}), ..., f_n(X_{n+1}), f_{n+1}(X_{n+1})\right] \tag{2}$$

where $X_{n+1} = (x_1, x_2, ..., x_n, x_{n+1})$. These functions $f(X_{n+1})$ verify the Cauchy-Riemann's conditions at $(n + 1)$D:

$$\begin{aligned} &\nabla \cdot f(X_{n+1}) = \sum_{j=1}^{n+1} \frac{\partial f_j(X_{n+1})}{\partial x_j} = 0 \\ &\frac{\partial f_j(X_{n+1})}{\partial x_k} - \frac{\partial f_k(X_{n+1})}{\partial x_j} = 0, 1 \le j,k \le n \ . \end{aligned} \tag{3}$$

By applying the Fourier Transform to the Eq. 3 (see the Appendix), we obtain the *n*D RT in the space domain (Stein and Weiss, 1971):

$$R_n f(X_{n+1}) = -\frac{x_n}{2\pi \left\| X_n \right\|^{n+1}} * f(X_{n+1}) \tag{4}$$

where the asterisk (*) represents convolution and $\|X_n\|^{n+1} = \sqrt{(x_1^2 + x_2^2 + ... + x_n^2)^{n+1}}$.

2.2. Monogenic signal extended to nD

In this paper, to represent the *n*D monogenic signal in a vectorial form, we are using a vector field $\mathbf{F}_n(X_{n+1})$ with $(n+1)$D. Detailed mathematical development of the *n*D monogenic signal may be found in (Sommer and Zang, 2007):

$$\mathbf{F}_n(X_{n+1}) = \sum_{j=1}^{n} f_j(X_{n+1})\mathbf{e}_j + f_{n+1}(X_{n+1})\mathbf{e}_{n+1} \tag{5}$$

where $f_j(X_{n+1}), f_{n+1}(X_{n+1})$ are monogenic components, and $(\mathbf{e}_j, \mathbf{e}_{n+1})$ are orthogonal bases (Sommer and Zang, 2007). By using the definition of the RT in Eq. 5, the solution to the problem of Neumann (Felsberg and Sommer, 2004) in a space, leads to the definition of the monogenic components of vector field $\mathbf{F}_n(X_{n+1})$ having $(n+1)$D with $X_{n+1}<0$ and $1 \le j \le n$ (see the Appendix):

$$\begin{aligned} f_j(X_{n+1}) &= f_j(X_n, x_{n+1}) = \frac{-x_j}{2\pi\|X_n\|^{n+1}} * f_{n+1}(X_n, x_{n+1}) = R_j f_{n+1}(X_n, x_{n+1}) \\ f_{n+1}(X_{n+1}) &= f_{n+1}(X_n, x_{n+1}) , \qquad 1 \le j \le \mathrm{n} \end{aligned} \tag{6}$$

where $X_{n+1} = (X_n, x_{n+1})$. Letting x_{n+1} tend to zero in the Eq. 6 yields an integral, which can be evaluated in a principal value sense (Felsberg *et al*., 2005; Sommer and Zang, 2007). We can deduce the space expression form of the *n*D RT and apply the Fourier Transform to the monogenic signal, which equations are written:

$$f(X_{n+1}) = -\frac{x_n}{2\pi\|X_n\|^{n+1}} * f(X_{n+1}) \tag{7}$$

$$\begin{aligned} f_j(X_n, 0) &= \frac{-x_j}{2\pi\|X_n\|^{n+1}} * f_{n+1}(X_n, 0) = R_j f_{n+1}(X_n, 0) \\ f_{n+1}(X_n, 0) &= f_{n+1}(X_n, 0) , \qquad 1 \le j \le \mathrm{n} \end{aligned}$$

using the two previous Eqs. 5 and 7, we obtain:

$$\mathbf{F}_n(X_n, x_{n+1}) = \sum_{j=1}^{n} R_j f_{n+1}(X_n, x_{n+1})\mathbf{e}_j + f_{n+1}(X_n, x_{n+1})\mathbf{e}_{n+1} \tag{8}$$

Eq. 8 represents a general mathematical formulation of the *n*D monogenic signal with the components of the operator of the RT $\sum_{j=1}^{n} R_j$ according to the axes $\sum_{j=1}^{n} \mathbf{e}_j$ respectively.

2.3. Case 2D monogenic signal

We use Eq. 8 to obtain a 2D monogenic signal with three components under the form (Sommer and Zang, 2007; Hidalgo-Gato and Barbosa, 2015; Li and Pilkington, 2016):

$$\mathbf{F}_2(X) = f(X)\mathbf{e}_z + R_x f(X)\mathbf{e}_x + R_y f(X)\mathbf{e}_y \tag{9}$$

where $X = (x, y, z)$, $(\mathbf{e}_x, \mathbf{e}_y, \mathbf{e}_z)$ are orthogonal bases, and (R_x, R_y) the two components of the RT (Fig. 1), according to two horizontal directions $(o\mathbf{e}_x, o\mathbf{e}_y)$ respectively. In this RT method, the RASA

and RLP are given via the following Eqs. 10 and 11, respectively (Felsberg and Sommer, 2001; Hidalgo-Gato and Barbosa, 2015):

$$RASA = R = \sqrt{f^2 + (R_x f)^2 + (R_y f)^2} \tag{10}$$

and

$$RLP = \tan^{-1}\left(\frac{\sqrt{(R_x f)^2 + (R_y f)^2}}{f}\right). \tag{11}$$

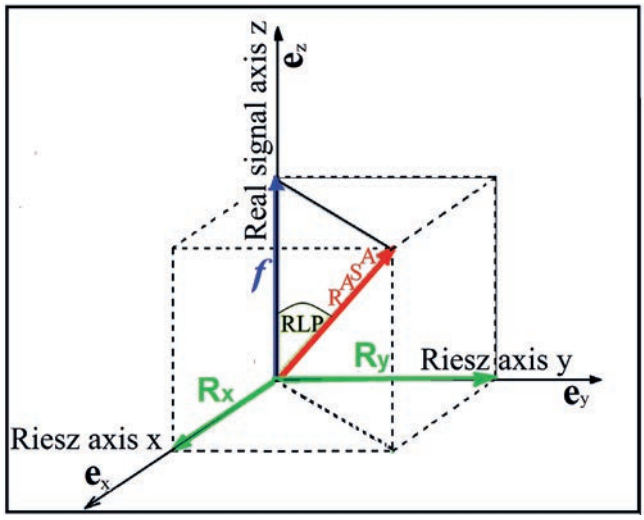

Fig. 1 - Representation of the 2D monogenic signal with three components, the component f is the real signal, and the components R_x and R_y are the x and y components of the first-order RT of the real signal.

The ASA and the Tilt Angle (TA) of the potential field T are given via Eqs. 12 and 13 below, respectively (Roest *et al*., 1992; Miller and Singh, 1994; Keating and Pilkington, 2004):

$$ASA = \sqrt{\left(\frac{\partial T}{\partial x}\right)^2 + \left(\frac{\partial T}{\partial y}\right)^2 + \left(\frac{\partial T}{\partial z}\right)^2} \tag{12}$$

and

$$TA = \tan^{-1}\left(\frac{\frac{\partial T}{\partial z}}{\sqrt{\left(\frac{\partial T}{\partial x}\right)^2 + \left(\frac{\partial T}{\partial y}\right)^2}}\right) \tag{13}$$

where ($\partial T / \partial x$, $\partial T / \partial y$, $\partial T / \partial z$) are first order derivatives of the potential field T in the x, y and z directions respectively.

2.4. Euler deconvolution using RASA

In this study, the RASA = R can replace the potential field *T*. By applying the *R* to Euler's homogeneity equation (Thompson, 1982; Reid *et al*., 1990; Cooper and Whitehead, 2016), we obtain:

$$(x-x_0)\frac{\partial R}{\partial x}+(y-y_0)\frac{\partial R}{\partial y}+(z-z_0)\frac{\partial R}{\partial z}=N(B-R) \tag{14}$$

where ($\partial R/\partial x, \partial R/\partial y, \partial R/\partial z$) are first order derivatives R in the *x, y,* and *z* directions respectively. The principle of the ED is based on the resolution of the preceding Eq. 14, which contains four unknown factors (x_0, y_0, z_0, and B). To solve a system of equations with four unknown factors, it will be necessary to have four points of measure. We consider a square window size $w \times w = n$ on the grids of the *R* gradients. This window gives a system of n linear equations. Solutions of the equation system in the sense of least squares are derived by resolving the inverse problem (Menke, 1989).

3. Monogenic signal using synthetic data

The RT method has been applied to a synthetic magnetic model composed of the vertical Dyke A and the dipping Dyke B, respectively (Fig. 2b). The vertical Dyke A is located at a position of 30 km and a depth of 2.5 km and has a magnetic susceptibility of 0.010 SI units, and magnetisation 1 A/m (Table 1). The second Dyke B has a depth of 5 km, the large depth extension to be regarded as infinite. The Dyke B is located at a position of 70 km (Fig. 2b); its magnetic susceptibility is 0.015 SI units, the magnetisation intensity 2 A/m and the dip is 60°E. The geomagnetic field has inclination of 30° and declination 10°W. The Total Magnetic Intensity (TMI) anomaly is calculated on a regular grid with a spacing of 1 km (Fig. 2a). The TMI anomaly was corrupted with pseudorandom zero-mean Gaussian noise with a standard deviation of 4 nT (Fig. 2c).

The calculation was made on the magnetic response to the synthetic model (Figs. 2d and 4a). By applying Eq. 11, the RLP values for the synthetic model are shown in Figs. 3d and 4d, respectively. In the ED method, the input synthetic magnetic data are derived from a dyke model. We are using SI = 1.25 and a moving window of 11×11 grid points for inversion (Barbosa *et al*., 1999; Beguiret *et al*., 2016; Harrouchi *et al*., 2016). The ED method has been applied to the

Table 1 - Physical parameters of the synthetic model.

Physical Parameters	Dyke A	Dyke B
Depth	2.5 km	5.0 km
Magnetic susceptibility	0.010 SI units	0.015 SI units
Magnetization	1 A/m	2 A/m
Total magnetic field	37,000 nT	37,000 nT
Declination	10°W	10°W
Inclination	30°	30°
Dip	90° (vertical)	60°E

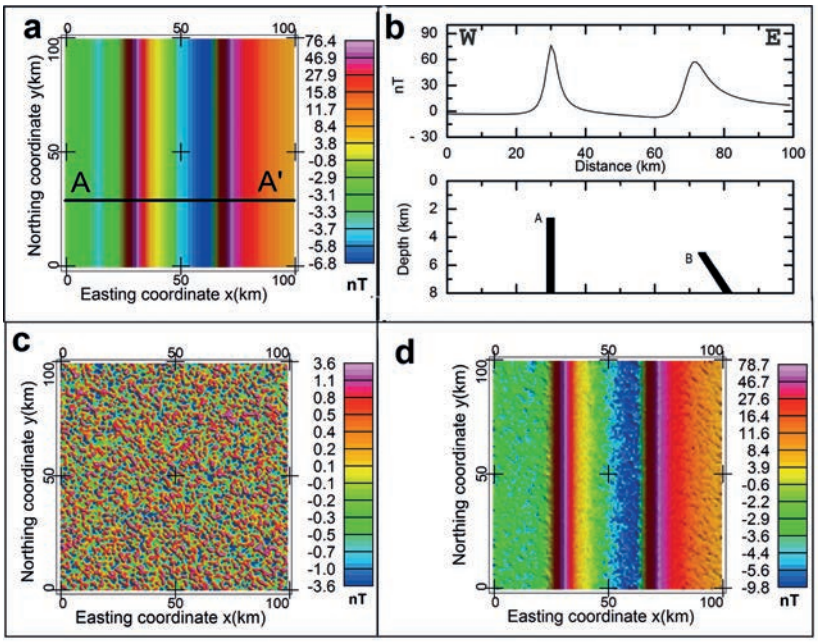

Fig. 2 - a) TMI anomaly map for the synthetic model described in the text, the inducing field has an inclination of 30° and a declination of -10°; b) TMI from the AA' profile marked in black solid line in Fig. 2a. The profile azimuth was west (left) to east (right). The data sampling interval was 1 km. The top of the vertical Dyke A is located at a depth of 2.5 km and the top of the dipping Dyke B at a depth of 5 km; c) Gaussian noise with standard deviation of 4 nT; d) Gaussian noise with standard deviation of 4 nT contaminated TMI anomaly from data in Fig. 2a.

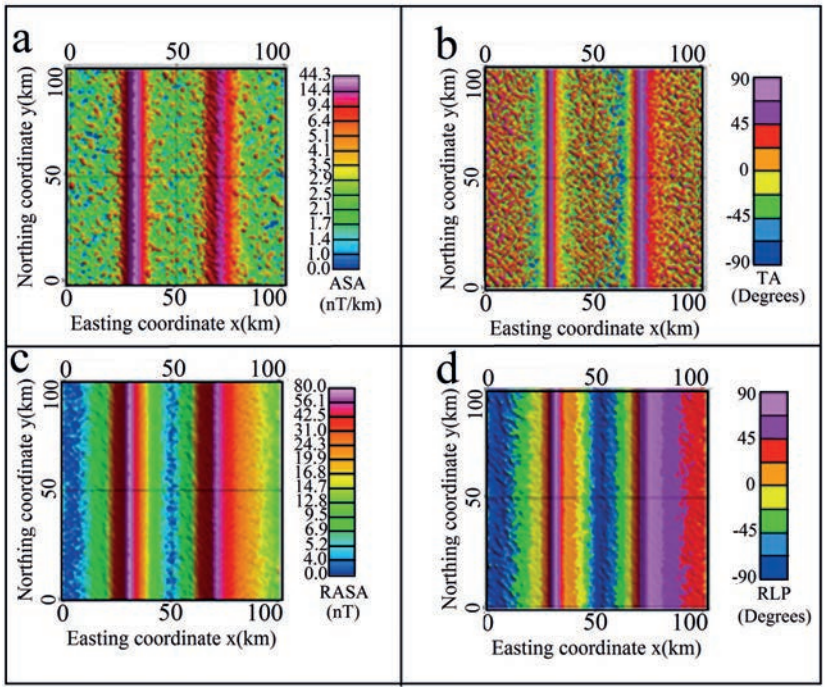

Fig. 3 - a) ASA of the data from Fig. 2d, obtained from Eq. 12; b) TA of the data from Fig. 2d, obtained from Eq. 13; c) RASA of the data from Fig. 2d, obtained from Eq. 10; d) RLP of the data from Fig. 2d, obtained from Eq. 11.

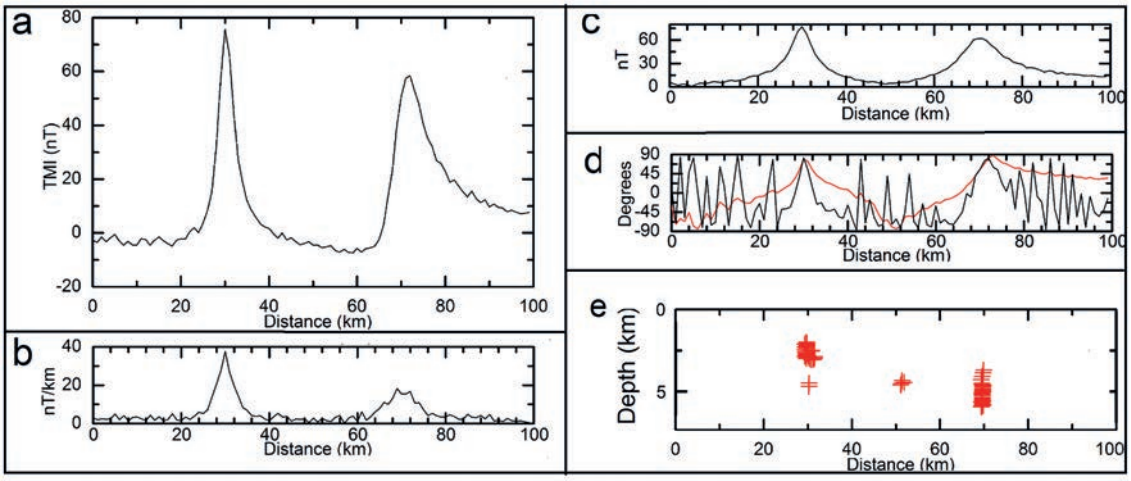

Fig. 4 - a) Zero-mean, Gaussian noise with 4 nT standard deviation contaminated TMI anomaly from AA' profile in Fig. 2b; b) ASA of the data from Fig. 4a; c) RASA of the data from Fig. 4a; d) TA (black solid line) of the data from Fig. 4c and the RLP (red solid line) of the data from Fig. 4c. We obtain the following results: RLP = 88° and RLP = 58° for vertical Dyke A and dipping Dyke B, respectively (Fig. 4d). The RLP is less sensitive to noise than the TA; e) depths obtained by the ED method (plotted in red), applied to the RASA from Fig. 4c, using N = 1.25 and a window size of 11×11 grid points.

RASA (Fig. 3c). We obtained the average depth of 2.53 km and 5.15 km for the Dyke A and B (Fig. 4e), respectively. We notice that the RT method is less sensitive to noise and gives a depth estimate close to the synthetic magnetic data (Figs. 3 and 4). Thus, we can apply this RT method to a real case of the study area.

4. Application to real data

The study area is located in southern Algeria (Fig. 5). It belongs to the Hoggar shield. It is represented by the paleoproterozoic basement corresponding to granulite facies (Caby, 1996). The granulite facies include quartzites, magnetite quartzites, marbles, calc-silicate gneisses, metadolomites (Fig. 5a), graphitic metapelites, and other gneisses possibly derived from greywackes, and of clear igneous origin, such as syenitic gneisses (Caby, 2003). During the regional metamorphism the temperature reached 1000°C in the study area (Ouzegane and Boumaza, 1996).

Fig. 5b shows Reduced To the Pole (RTP) aeromagnetic data from the central In Ouzzal terrane and adjacent zone. The field inclination is 27° and the declination is 4.7°W. The data sampling interval was 46.2 m (Aeroservice Corporation, 1975; Harrouchi *et al*., 2016). The RTP aeromagnetic data were upward continued by 0.5 km to remove short wavelength noise. The comparison between the geological map (Fig. 5a) and the RTP anomaly map (Fig. 5b) of the study area showed a good correlation, indicating that the magnetic structures, generally, follow the direction of the geological structures.

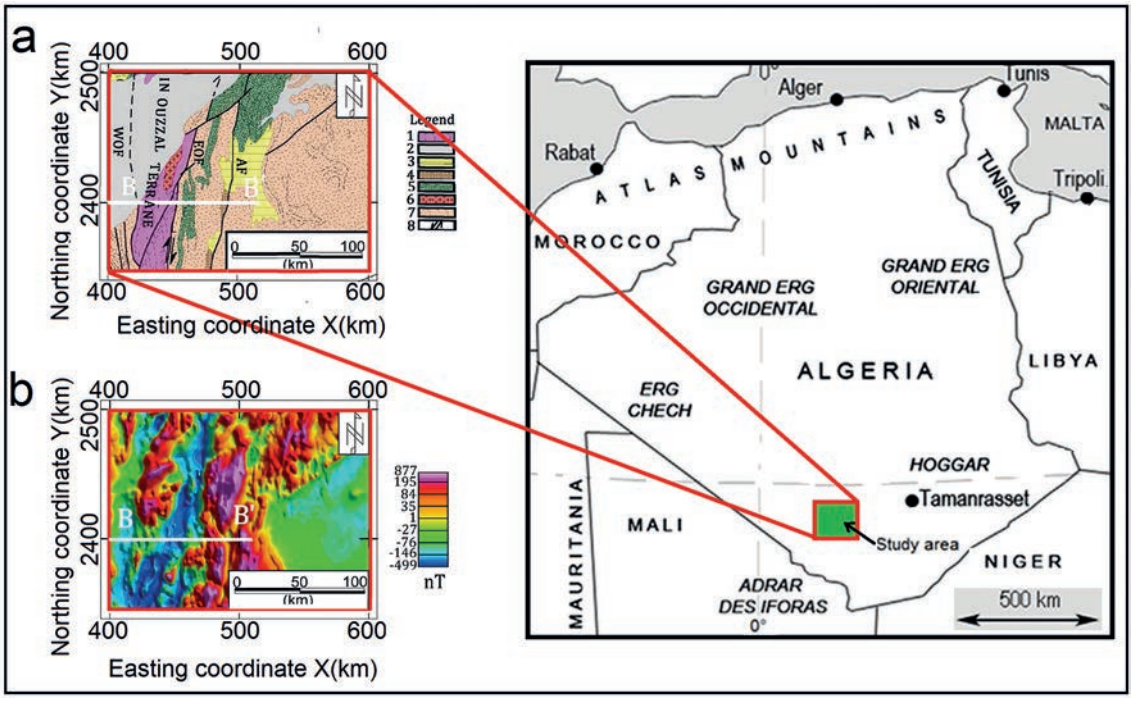

Fig. 5 - Location of the study area: a) geological map of the study area (after Caby, 1996): WOF (West Ouzzalian Fault), EOF (East Ouzzalian Fault), AF (Adrar Fault), 1 - granulitic unit, 2 - Paleozoic sediments, 3 - Cambrian molasse, 4 - Cambrian volcanics, 5 - Late Paleoproterozoic sediments and magmatics, 6 - granites intruding the IOGU (In Ouzzal Granulitic Unit), 7 - Panafrican metamorphics and granitoides, 8 - major shear zone; b) RTP aeromagnetic data from the study area. Location of aeromagnetic BB' profile (white solid line) cutting the central In Ouzzal terrane and adjacent zone.

5. Results and discussion

Fig. 6 represents the RT solution: the RASA (Fig. 6a) of the RTP aeromagnetic data from the study area (Fig. 5b), obtained from Eq. 10, the RLP of the same data, obtained from Eq. 11, respectively.

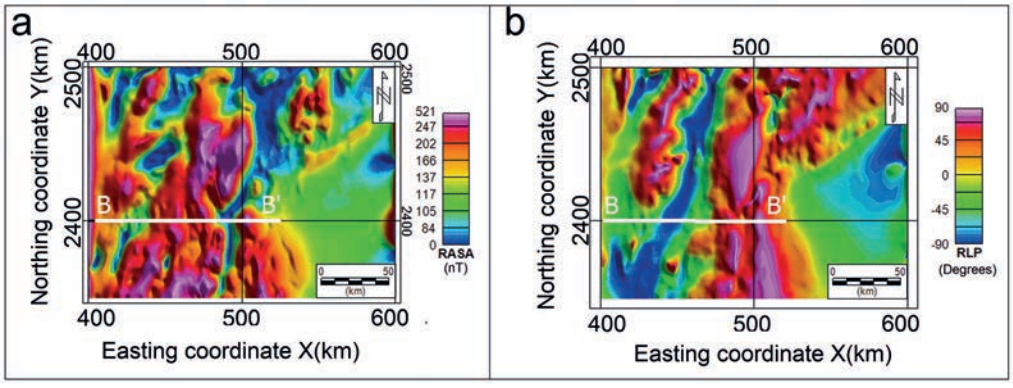

Fig. 6 - Solution from RT method of the study area; a) RASA of the data from Fig. 5b, obtained from Eq. 10; b) RLP of the data from Fig. 5b, obtained from Eq. 11.

Fig. 7 shows the interpretation of the BB' profile by three previous techniques (RASA, RLP, and ED), using the RT method (Table 2). The aeromagnetic data collected were subjected to mathematical processing (RTP, RASA and RLP) using the Oasis montaj software (Geosoft Inc., 2007).

Comparison of the results obtained by the interpretation of the BB' profile with the geological data of the study area (Fig. 5a) allows us to note the following: the WOF is below the Paleozoic cover and its depth and RLP are 0.8 km and -90° (vertical) respectively (Figs. 6b and 7c). At a distance of 30 km from the WOF (Fig. 7d), we find the EOF with a depth of about 5 km (Fig. 7d) and a RLP of -90° (vertical). At a distance of about 50 km further east of the EOF (Fig. 7d), we meet the Adrar Fault (AF) with a depth and a RLP of about 0.3 km and +90° (vertical), respectively (Table 2). The results of the interpretation of the fault systems (Fig. 7c) are summarised in Table 2.

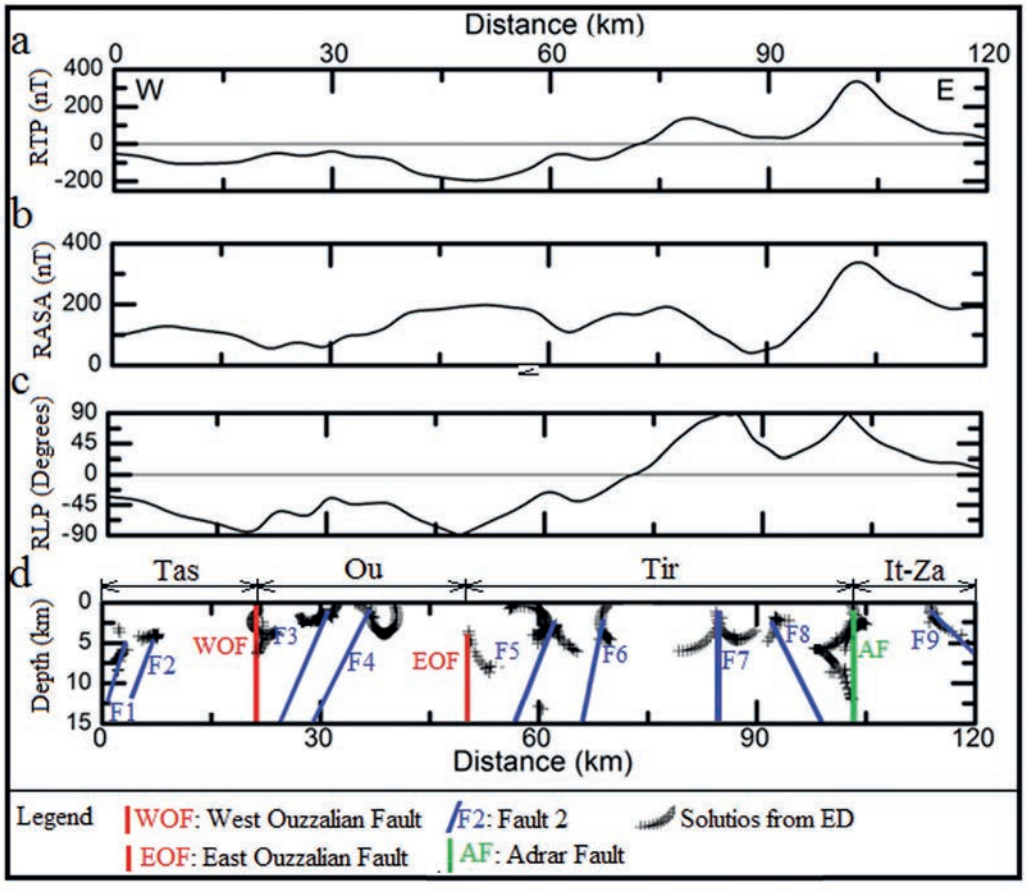

Fig. 7 - a) RTP aeromagnetic data from BB' profile, azimuth was west (left) to east; b) RASA from Fig. 7a is obtained from Eq. 10; c) RLP from Fig. 7b is obtained from Eq. 11; d) solutions from ED and from Fig. 7b, the SI N used is 1.25, and the window size is 11 samples; Tas (Tassendjanet terrane), Ou (In Ouzzal terrane), Tir (Tirek terrane), It-Za (In Teideni terrane - Tin Zaoutene terrane), WOF (West Ouzzalian Fault) and EOF (East Ouzzalian Fault) red solid line, AF (Adrar Fault) green solid line and F1, F2, …, F9 (fault system) blue solid line.

Table 2 - Estimated depth and RLP for BB' profile.

Localisation (km)	Depth (km)	RLP (degrees)	Magnetic source (Fault)
3.0	5.0	-35° (45°W)	F1
8.0	3.5	-45° (50°W)	F2
20.0	0.8	-90° (vertical)	WOF
30.0	2.0	-35° (45°W)	F3
37.0	1.0	-45° (45°W)	F4
50.0	5.0	-90° (vertical)	EOF
63.0	2.5	-25° (30°W)	F5
73.0	0.5	-20° (20°W)	F6
84.0	1.5	+90° (vertical)	F7
95.0	2.5	+15° (15°E)	F8
102.0	0.3	+90° (vertical)	AF
114.0	0.2	+15 (18°E)	F9

6. Conclusions

The application of the RT method to a synthetic magnetic model allowed us to note the following: 1) the advantage of this method is that it is less sensitive to noise; 2) it allows to obtain a better estimation of the geometric parameters (depth and dip). The application of the ED method using the RASA to the synthetic data example gave more valid results. By applying the RLP to the RTP aeromagnetic data from study area and adjacent zone of the In Ouzzal terrane, we obtained the WOF and the EOF dips, they are vertical. We confirmed that the RLP of the AF demonstrates the fault is vertical. The faults systems that are located inside of the central In Ouzzal terrane are inclined toward the west.

Acknowledgements. The authors would like to thank the Draria Nuclear Research Center, Algeria, for supplying geophysical data. Thanks to G.R.J. Cooper from University of the Witwatersrand, South Africa, for his help. Thanks to the Editor of BGTA for his kind cooperation and help.

REFERENCES

Aeroservice Corporation; 1975: *Aero-magneto-spectrometric survey of Algeria*. Aeroservice Corporation Houston - Philadelphia, TX - PA, USA, Final report, 3 vols.

Barbosa V.C.F., Joao B.C. and Medeiros W.E.; 1999: *Stability analysis and improvement of structural index estimation in Euler déconvolution*. Geophys., **64**, 48-60.

Beguiret L., Assassi F. and Harrouchi L.; 2016: *Deconvolution applied to aeromagnetic data of the Debbagh massive, neritic Constantinois (north-eastern Algeria)*. Boll. Geof. Teor. Appl., **57**, 247-260.

Blakely R.J.; 1995: *Potential theory in gravity and magnetic applications*. Cambridge University Press, Cambridge, England, 441 pp., doi: 10.1017/CBO9780511549816.

Bracewell R.N.; 1965: *The Fourier Transform and its applications*. McGraw-Hill, New York, NY, USA, 474 pp.

Bülow T.; 1999: *Hypercomplex spectral signal representation for the processing and analysis of images*. Ph.D. thesis, Institut für Informatik und Praktische Mathematik, Christian Albrechts University zu Kiel, Kiel, Germany, 161 pp.

Caby R.; 1996: *A review of the In Ouzzal granulitic terrane (Tuareg shield, Algeria): its significance within the Pan-African Trans-Saharan Belt*. J. Metamorph. Geol., 14, 659-666.

Caby R.; 2003: *Terrane assembly and geodynamic evolution of central-western Hoggar: a synthesis*. J. Afr. Earth Sci., **37**, 133-159.

Cooper G.R.J. and Whitehead R.C.; 2016: *Determining the distance to magnetic sources*. Geophys., **81**, J39-J48.

Durrheim R.J. and Cooper G.R.J.; 1998: *Euler deconvolution of magnetic and gravity data*. Comput. Geosci., **24**, 545-550.

Felsberg M. and Sommer G.; 2001: *The monogenic signal*. IEEE Trans. Signal Process., **49**, 3136-3144, doi: 10.1109/78.969520.

Felsberg M. and Sommer G.; 2004: *The monogenic scale-space: a unifying approach to phase-based image processing in scale-space*. J. Math. Imaging Vision, **21**, 5-26, doi: 10.1023/B:JMIV.0000026554.79537.35.

Felsberg M., Duits R. and Florack L.; 2005: *The monogenic scale space on a rectangular domain and its features*. Int. J. Comput. Vision, **64**, 187-201, doi: 10.1007/s11263-005-1843-x.

Geosoft Inc.; 2007: *Oasis montaj*. <www.geosoft.com/media/uploads/resources/brochures/OM_b_2008_10_web.pdf.>.

Harrouchi L., Hamoudi M., Bendaoud A. and Beguiret L.; 2016: *Application 3D Euler deconvolution and improved tilt angle to the aeromagnetic data of In Ouzzal terrane, western Hoggar, Algeria*. Arabian J. Geosci., **9**, 508-518, doi: 10.1007/s12517-016-2536-1.

Hassan H. and Yalamanchili S.V.; 2013: *Monogenic signal decomposition: a new approach to enhance magnetic data*. In: Expanded Abstracts, 83rd Annual International Meeting SEG, Houston, TX, USA, pp. 1206-1210.

Hidalgo-Gato M. and Barbosa V.C.F.; 2015: *Edge detection of potential-field sources using scale-space monogenic signal: fundamental principles*. Geophys., **80**, J27-J36.

Keating P. and Pilkington M.; 2004: *Euler deconvolution of the analytic signal and its application to magnetic interpretation*. Geophys. Prospect., **52**, 165-182, doi: 10.1111/j.1365-2478.2004.00408.x.

Li X. and Pilkington M.; 2016: *Attributes of the magnetic field, analytic signal and monogenic signal for gravity and magnetic interpretation*. Geophys., **81**, J79-J86.

Menke W.; 1989: *Geophysical data analysis: discrete inverse theory, 3rd ed*. Academic Press Inc., Cambridge, MA, USA, 330 pp.

Miller H.G. and Singh V.; 1994: *Potential field tilt - a new concept for location of potential field sources*. J. Appl. Geophys., **32**, 213-217.

Nabighian M.N.; 1984: *Toward a three-dimensional automatic interpretation of potential field data via generalized Hilbert transforms: fundamental relations*. Geophys., **49**, 780-786.

Ouzegane K. and Boumaza S.; 1996: *An example of ultrahigh-temperature metamorphism: orthopyroxene-sillimanite-garnet, sapphirine-quartz and spinel-quartz parageneses in Al-Mg granulites from In Hihaou, In Ouzzal, Hoggar*. J. Metamorph. Geol., **14**, 693-708.

Reid A.B., Allsop J.M., Granser H., Millet A.J. and Somerton I.W.; 1990: *Magnetic interpretation in three dimensions using Euler deconvolution*. Geophys., **55,** 80-91.

Riesz M.; 1928: *Sur les fonctions conjuguées*. Math. Z., **27**, 218-244, doi: 10.1007/BF01171098.

Roest W.R., Verhoef J. and Pilkington M.; 1992: *Magnetic interpretation using the 3-D signal analytic*. Geophys., **57**, 116-125.

Sommer G. and Zang D.; 2007: *Parity symmetry in multi-dimensional signals*. Commun. Pure Appl. Anal., **6**, 829-852, doi: 10.3934/cpaa.2007.6.829.

Stein E.W. and Weiss G.; 1971: *Introduction to Fourier analysis on Euclidean spaces*. Princeton University Press, Princeton, NJ, USA, 297 pp.

Thompson D.T.; 1982: EULDPH: *a new technique for making computer-assisted depth estimates from magnetic data*. Geophys., **47**, 31-37.

Corresponding author: Lakhdar Harrouchi
Sahara Geology Laboratory, Kasdi Merbah University
P.O. Box 511, Ouargla 30000, Algeria
Phone: +213 66 6323288; e-mail: Harrouchi_lakhdar@yahoo.fr

Appendix: *n*D Riesz Transform in the space domain

The derivation functions $f(X_{n+1})$ are equivalent to the concept of *n*D harmonic field related to the equation of Laplace $\Delta p = 0$; where p is scalar potential (Blakely, 1995). One can thus easily move to higher dimensions using Laplacian (*n*+1)D:

$$\nabla f(X_{n+1}) = \Delta p\ (X_{n+1}) \tag{A1}$$

where ∇, = (∂ / ∂x_1, ∂ / ∂x_2, ..., ∂ / ∂x_n, ∂ / ∂x_{n+1}) and $\Delta = \nabla^2$. The generalisation of Cauchy-Riemann's conditions at (n+1)D via the two following Eqs.:

$$divf(X_{n+1}) = \nabla \cdot f(X_{n+1}) = \sum_{j=1}^{n} \frac{\partial f_j(X_{n+1})}{\partial x_j} + \frac{\partial f_{n+1}(X_{n+1})}{\partial x_{n+1}} = 0 \tag{A2}$$

$$rotf(X_{n+1}) = \nabla \times f(X_{n+1}) = \frac{\partial f_j(X_{n+1})}{\partial x_k} - \frac{\partial f_k(X_{n+1})}{\partial x_j} = 0 \quad , \ 1 \le j,k \le n \tag{A3}$$

By applying the properties of the derivation of Fourier Transform to the Conditions of Riemann (Eq. A3), we obtain (Bracewell, 1965):

$$\sum_{j=1}^{n} i2\pi \|U_n\| F_n(U_n, x_{n+1}) + \frac{\partial F_{n+1}(U_n, x_{n+1})}{\partial x_{n+1}} = 0 \tag{A4}$$

where $i^2 = -1$, $U_n = (u_1, u_2, ..., u_n)$ and $F_n(U_n, x_{n+1}) = \nabla P(U_n, x_{n+1})$, we can, therefore, write:

$$\frac{\partial^2 P(U_n, x_{n+1})}{\partial x^2_{n+1}} = 4\pi^2 \|U_n\|^2 P(U_n, x_{n+1}) \ . \tag{A5}$$

The solution of Eq. A5 is given by (Felsberg and Sommer, 2001):

$$P(U_n, x_{n+1}) = C(U_n) \exp\ (2\pi \|U_n\| x_{n+1}) \tag{A6}$$

where $C(U_n)$ is an independent function of x_{n+1} and $\|U_n\| = \sqrt{u_1^2 + u_2^2 + ... + u_n^2}$, we apply the conditions of Riemann (n+1)D to Eq. A6 we obtain:

$$\begin{aligned} &F_k(U_n, x_{n+1}) = i2\pi\ u_n P(U_n, x_{n+1}), \quad 1 \le k \le n \\ &F_{n+1}(U_n, x_{n+1}) = \frac{\partial P(U_n, x_{n+1})}{\partial x_{n+1}} = 2\pi \|U_n\| C(U_n) P(U_n, x_{n+1}) \end{aligned} \tag{A7}$$

From Eq. A7, one can easily draw the value of $F_k(U_n, x_{n+1})$:

$$F_k(U_n, x_{n+1}) = i \frac{u_k}{\|U_n\|} O(U_n) F_{n+1}(U_n, x_{n+1}) \tag{A8}$$

If $x_{n+1} \to 0$, we obtain the Eq. A8 by:

$$F_k(U_n, 0) = i \frac{u_k}{\|U_n\|} O(U_n) F_{n+1}(U_n, 0) \tag{A9}$$

where $O(U_n) = 1/C(U_n)$. Eq. A9 represents the RT in the frequency domain. By applying the Fourier Transform to Eq. A9, we obtain a mathematical formulation of the nD RT in the space domain (Stein and Weiss, 1971).